Chapter 3

Pre-processing

This chapter describes preprocessing of the image data. Broken down into two sections, we consider geometric registration and radiometric normalization. The two sections in this chapter provide the details of these steps. The essential results from these two sections, as they pertain to the main study, are contained in the "Essential Results" subsection at the end of each section.

For both geometric registration and radiometric correction, we believed pre-processing should be as straightforward as possible. We wish to maintain the characteristics of the data as it arrived from Eosat and use methods that require no special data (i.e. in situ atmospheric measurements). We believe this approach will help make the proposed change detection method more generally applicable and accessible to a wider group of possible users by using readily available satellite data and standard preprocessing algorithms.

Geometric Correction

Overview

Studies have shown the importance of proper registration for image-based change detection. In their review of accuracy assessment of satellite derived land-cover data, in the section on positional accuracy, Janssen and van der Wel (1994) stress the importance of registration considerations. Coppin and Bauer (1996) and Dobson *et al.* (1995) describe its importance for image change detection. Chrisman (1991) presents a detailed description of positional accuracy as a component of error. Townshend *et al.* (1992)

discuss the impact of misregistration on change detection and conclude the effects can be significant. (In their particular case, they find misregistration leading to overestimates of changes in the Normalized Difference Vegetation Index.) All of these studies highlight the importance of proper geometric registration for image-based change detection. While all of the TM data acquired were geocoded, for pixel specific comparison between two dates, geometric correction was needed to ensure that the 1994 and 1988 images were properly registered to each other.

The generally accepted procedure for geometric registration is to match a set of points on one image to those on the other. The coordinates from this set of points are then used to calculate a transformation function that will change the coordinates of one image so it will more closely match, geometrically, the other image (Jensen, 1996, chapter 6; Richards 1993, section 2.5; Lillesand and Kiefer, 1994, section 7.2). This is referred to as ground control point (GCP) registration. It is the registration method recommended by the NOAA C-CAP program (Dobson, *et al.*, 1995). In light of findings showing the error associated with positional accuracy of USGS quad sheets (Cook, 1996), and following the logic suggested by the Earth Satellite Corporation (FGDC, 1992) we register one image to another and match subsequent images and/or digital maps to that same master image. This also follows the C-CAP protocol for rectification of multiple images (Dobson *et al.*, 1995, p. 15). We will use the ’94 images as the masters. First we describe how the 1988 imagery was rectified to the 1994 imagery and then how the 1994 Digital Orthophoto Quarter Quadrangles (DOQQ) and the ancillary data were checked against the 1994 TM data.

Geometric rectification of 1988 Thematic Mapper imagery to 1994 Thematic Mapper imagery

The generally accepted measure of positional accuracy is “Root mean square error” or RMS error, which is the square root of the sum of squared individual error terms (Jensen, 1996, p. 129). It is recommended by the NOAA C-CAP program (Dobson *et al.*, 1995) and others (Khorram, in press, p.24) that the root mean square error (RMSE) be less than

1/2 pixel. Giving a bit more allowance, the Federal Geographic Data Committee find RMS errors of .5 to 1 pixel are low enough to allow pixel by pixel change detection analysis (FGDC, 1992). Fortunately, geocoded Landsat data has reportedly been relatively easy to rectify (Khorram, in press, p. 24). We used RMSE of one-half pixel as our criteria for geometric correction.

Our image-to-image registration was done within Imagine™ software using the "GCP Editor" (ground control point editor). By linking the 1988 data as the "source image" to the 1994 image as the "destination" image we used Imagine™ to register the 1988 image to the 1994 image through three steps:

1. selecting ground control points on each image which represent the same ground location
2. selecting a transformation matrix which will convert the coordinates of the 1988 image to match the 1994 image
3. applying that transformation to the 1988 image through Imagine's™ resampling module.

Each of these three steps was conducted separately for the coastal and Raleigh images. Thirty-one points were collected for the coastal scenes and thirty points were found for the Raleigh images. Most ground control point were at road intersections - either with other roads or with noticeable features, or from constructed surfaces which were distinguishable by being surrounded by vegetation. The use of water/land edges was not used as shorelines can shift over time. Also avoided were corners or edges of one vegetation type to the next. This was because vegetation edges can change or drift over time or the spectral response on this type of boarder is such that the edge tends to be blurred.

For both scenes a first order, affine, transformation was sufficient and resulted in root-mean-square errors (RMSE) in the X and Y direction less than half a pixel. (That is, less than 14.25 meters = 1/2 x 28.5 meters. Here "X" refers to the East-West direction and "Y" to the North-South.) The affine transformation is a linear transformation where the new "X" values for 1988 are based on a linear function of the "X" and "Y" values from

1994. Likewise the new "Y" values are based on a linear function of the "X" and "Y" values from 1994. The coefficients for the affine transformation for the coastal scene are given in table 3.1 and table 3.2 for the Raleigh scene. To test whether or not to go from an affine to a higher order transformation, the GCP coordinates were brought into SAS™ software. Statistics from this analysis are presented in table 3.3. First, note that the RMSE for the affine transformation is below a half pixel for each scene in either direction. Looking at the "Reduction in RMSE" column" we find higher order transformations did not reduce the RMSE in the Y (East-West) direction for either scene and produced only slight improvements in the X (North-South) direction. Since the affine transformation model is a subset of the higher order polynomial models we can test the improvement in the higher order model using a standard F test to compare full and reduced models (Neter *et al.*, 1989, section 3.9):

$$F = \frac{SSE(R) - SSE(F)}{df_R - df_F} \div \frac{SSE(F)}{df_F} \qquad \textbf{(eq. 3.1)}$$

where ***SSE(.)*** is the sum of squares, ***df*** represents the degrees of freedom, and ***R*** and ***F*** represent full and reduced. For our test the full model is the second order transformation and the reduced model is the affine transformation. Table 3.3 lists this F statistic as well as the p-value. Only the p-value for the coastal image X direction gives an indication of an improvement from the second order model. However, while there is statistically significant improvement, there is only a slight practical improvement of 1.64 meters. Considering the practical improvement and for consistency we used the simpler, first order, affine, transformation for both images in both directions.

Table 3.1: Coastal area image registration transformation matrix and resulting RMS error

	x	y
const	19.139603	-247.28732
x	0.999879	0.000279
y	0.000638	0.999867

Table 3.2: Raleigh area image registration transformation matrix and resulting RMS error

	x	y
const.	417.37135	368.56474
x	0.999612	-0.000546
y	-0.000795	0.999756

Table 3.3: Reduction in RMSE and F-test for significance of second order transformations

	Affine transformations transformation			**Second order transformation**			Reduction in RMSE:		
	SSE(R)	df(R)	RMSE	SSE(F)	df(F)	RMSE	RMSE(R) - RMSE(F)	F statistic	p-value
coast X	3551.89	28	11.26	2315.74	25	9.62	1.64	4.45	0.01
coast Y	4177.15	28	12.21	3953.34	25	12.58	-0.36	0.47	0.70
Raleigh X	1223.85	27	6.73	1004.20	24	6.47	0.26	1.75	0.18
Raleigh Y	1274.15	27	6.87	1225.01	24	7.14	-0.27	0.32	0.81

The listing of the individual ground control points are given in table 3.4 for the coast and 3.5 for Raleigh. Tables 3.4 and 3.5 list the X and Y coordinates for the 1988 image as the "source" and the X and Y coordinates for the 1994 image as the "destinations". The coordinates represent units in State Plane Meters (as described in Chapter 2). The "residual" column lists the difference in the source and destination coordinates after the transformation has been applied to the source data. The "RMS Error" column is the square root of the sum of the squared residuals. The "Contribution" column gives the ratio of that point's RMS Error divided by the total RMSE (Erdas, 1994, pp. 304-305). There are generally larger deviations, and resulting higher RMSE, for the coastal scene. This may be due to constructed features in the coastal scene tending to be smaller and surrounded by more vegetation. As this vegetation can grow or die-back over the course of six years, this may have caused the larger errors in some of the coastal scene ground control points.

Table 3.4: Coastal area ground control points

Row	X Source	Y Source	X Dest.	Y Dest.	X Resid.	Y Resid.	RMS Error	Contri-bution
1	802,276.034	131,471.378	802,289.570	131,502.931	19.569	-9.777	21.875	1.385
2	803,386.877	131,983.523	803,387.412	132,045.108	6.781	20.488	21.581	1.367
3	800,352.716	132,170.593	800,338.329	132,211.051	-7.667	-1.511	7.815	0.495
4	797,344.567	130,956.166	797,352.143	130,995.088	13.881	-3.717	14.370	0.910
5	809,314.431	132,070.925	809,315.470	132,125.218	6.620	14.837	16.247	1.029
6	816,710.867	130,220.150	816,697.311	130,242.621	-10.070	-14.677	17.799	1.127
7	812,278.208	129,703.405	812,278.785	129,734.778	4.274	-6.939	8.150	0.516
8	821,259.813	132,320.863	821,253.067	132,378.425	-2.448	21.397	21.536	1.364
9	801,559.954	125,202.971	801,560.535	125,231.423	2.701	-12.245	12.540	0.794
10	799,050.613	126,811.474	799,054.655	126,853.661	7.500	0.576	7.522	0.476
11	808,518.786	126,846.741	808,517.820	126,876.550	1.362	-9.170	9.271	0.587
12	813,644.574	125,285.773	813,616.779	125,310.103	-27.083	-13.019	30.049	1.903
13	814,929.847	123,065.456	814,929.043	123,094.189	-1.664	-7.955	8.128	0.515
14	821,027.240	125,029.700	821,010.055	125,066.910	-17.521	1.953	17.629	1.116
15	820,780.896	126,860.541	820,769.902	126,898.008	-10.133	1.898	10.309	0.653
16	804,128.969	120,713.270	804,130.742	120,742.374	0.719	-10.280	10.305	0.653
17	801,608.917	117,733.937	801,599.131	117,762.549	-12.435	-11.079	16.654	1.055
18	806,266.499	116,441.308	806,264.957	116,483.642	-5.570	4.113	6.924	0.439
19	805,241.341	118,445.420	805,238.590	118,500.710	-5.369	16.515	17.366	1.100
20	814,727.875	115,878.562	814,727.486	115,937.174	-5.790	22.821	23.545	1.491
21	821,625.504	119,672.114	821,649.033	119,710.951	19.700	4.472	20.201	1.279
22	798,369.724	111,180.324	798,372.792	111,236.404	-3.354	16.361	16.701	1.058
23	801,648.699	112,290.482	801,663.458	112,349.368	8.649	19.935	21.730	1.376
24	802,646.315	112,633.956	802,648.370	112,661.226	-3.975	-11.448	12.118	0.767
25	808,604.471	111,008.587	808,603.589	111,037.558	-8.668	-7.871	11.708	0.741
26	805,865.616	114,027.787	805,866.132	114,054.577	-5.014	-11.218	12.288	0.778
27	817,322.902	113,486.509	817,321.994	113,515.262	-8.167	-5.992	10.129	0.641
28	823,593.195	111,692.468	823,620.288	111,724.220	17.930	-1.000	17.958	1.137
29	824,194.518	112,039.010	824,217.811	112,063.259	14.274	-8.381	16.552	1.048
30	820,641.658	110,223.502	820,656.973	110,263.633	5.579	6.749	8.756	0.555
31	824,391.900	114,003.254	824,405.073	114,030.258	5.387	-5.836	7.942	0.503

Table 3.5 Raleigh area ground control points

Row	X Source	Y Source	X Dest.	Y Dest.	X Resid.	Y Resid.	RMS Error	Contri-bution
1	629,623.695	237,720.578	629,650.907	237,747.171	11.209	-6.660	13.038	1.429
2	629,962.372	234,981.051	629,973.034	235,013.808	-3.293	-0.005	3.293	0.361
3	627,458.580	240,402.591	627,465.704	240,429.400	-10.163	-5.904	11.753	1.288
4	623,643.926	240,223.992	623,660.570	240,258.953	0.970	4.367	4.473	0.490
5	630,939.093	238,407.731	630,961.099	238,449.107	4.937	7.237	8.761	0.960
6	636,695.093	235,491.118	636,722.229	235,523.602	10.156	-4.087	10.948	1.200
7	643,332.560	237,520.790	643,359.918	237,575.174	6.170	13.688	15.015	1.645
8	639,173.181	237,887.069	639,198.586	237,925.367	5.554	-0.212	5.558	0.609
9	646,989.971	239,212.940	647,008.634	239,257.959	-5.279	1.920	5.617	0.616
10	627,141.070	230,307.206	627,146.673	230,340.438	-3.540	3.154	4.741	0.520
11	627,788.185	232,961.975	627,798.672	232,990.127	-1.016	-2.928	3.099	0.340
12	629,162.549	230,989.818	629,177.007	231,016.031	3.989	-5.138	6.505	0.713
13	634,923.085	227,514.705	634,924.199	227,543.544	-8.826	-4.803	10.048	1.101
14	633,184.341	229,181.125	633,185.019	229,226.329	-9.924	12.101	15.650	1.715
15	643,002.955	231,832.866	643,019.206	231,860.523	-0.262	-11.459	11.462	1.256
16	644,746.235	229,642.758	644,756.837	229,680.340	-4.853	-1.950	5.230	0.573
17	647,189.549	226,735.226	647,203.769	226,773.430	0.126	-1.956	1.960	0.215
18	625,538.401	225,153.566	625,542.230	225,172.770	-0.585	-8.737	8.757	0.960
19	629,594.968	222,631.990	629,595.154	222,665.637	-3.808	4.105	5.599	0.614
20	636,607.399	222,075.003	636,615.369	222,114.006	1.689	5.761	6.004	0.658
21	633,146.542	224,160.676	633,157.143	224,182.623	4.018	-9.911	10.695	1.172
22	641,265.722	222,149.167	641,280.026	222,188.383	6.153	3.409	7.035	0.771
23	645,109.103	220,375.286	645,105.293	220,425.023	-12.045	12.272	17.195	1.884
24	646,066.169	222,283.873	646,067.030	222,323.192	-9.255	0.865	9.295	1.019
25	650,671.573	220,045.332	650,683.677	220,079.479	1.979	-6.280	6.584	0.722
26	624,693.220	215,501.652	624,691.998	215,530.071	2.358	3.295	4.052	0.444
27	624,691.708	212,812.072	624,688.901	212,838.545	2.914	2.007	3.538	0.388
28	644,015.962	217,900.630	644,015.014	217,944.232	-6.787	7.338	9.995	1.095
29	648,122.423	215,684.792	648,139.178	215,717.564	11.085	-5.201	12.245	1.342
30	649,059.833	214,803.905	649,071.490	214,835.883	6.326	-6.289	8.920	0.978

For further analysis of the ground control points, figures 3.1 and 3.4 show the spatial location of the points and the magnitude of the individual RMS Errors. Each ground control point has a corresponding circle. The diameter of the circle is proportional to the RMS Error for that point. So, larger circles indicate greater error. (Note, the circles are not to scale and do not represent meters.) An optimal set of ground control points would be well distributed over the study area and the magnitude of error should not show any spatial pattern. From figures 3.1 through 3.4 we see there is no clear spatial pattern in the size of error and that the CGP are fairly uniformly distributed over the images.

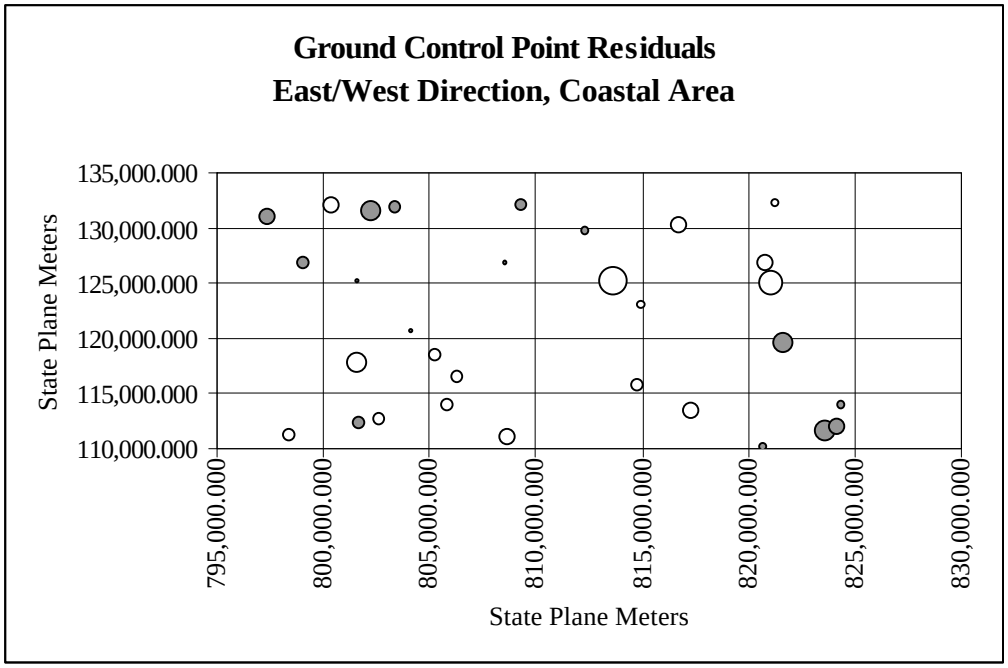

Gray circles represent positive residuals
White circles represent negative residuals

Figure 3.1: Distribution and magnitude of East/West residuals for the coastal area

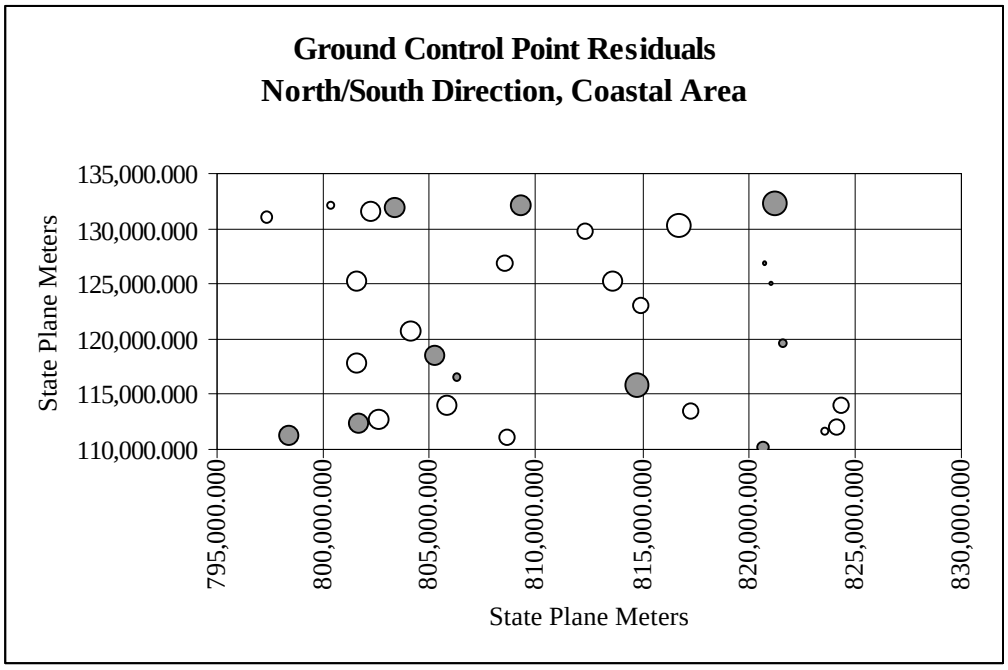

Figure 3.2: Distribution and magnitude of North/South residuals for the coastal area

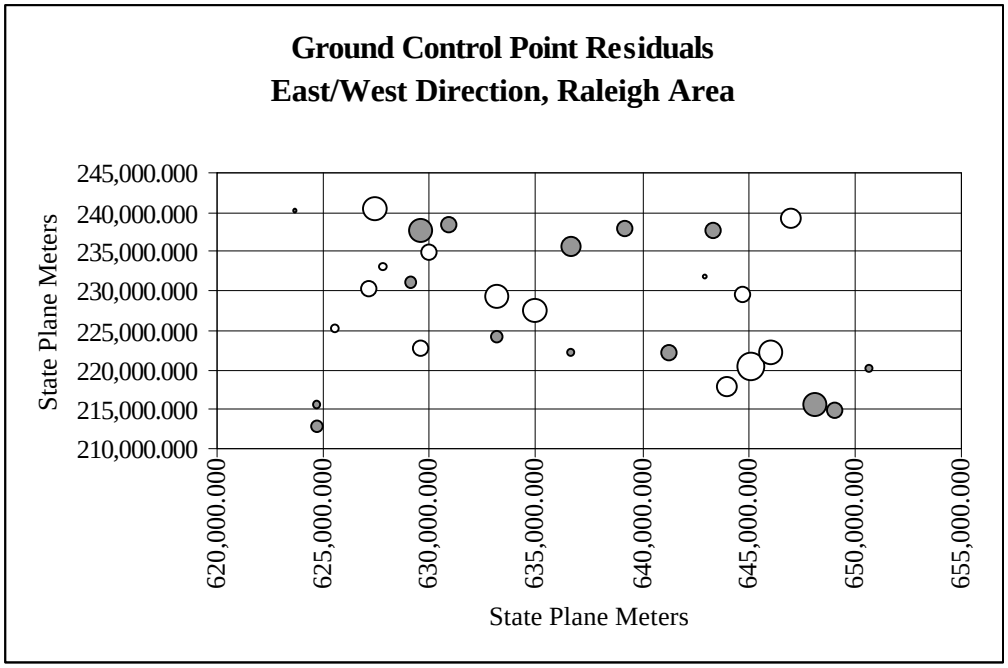

Figure 3.3: Distribution and magnitude of East/West residuals for the Raleigh area

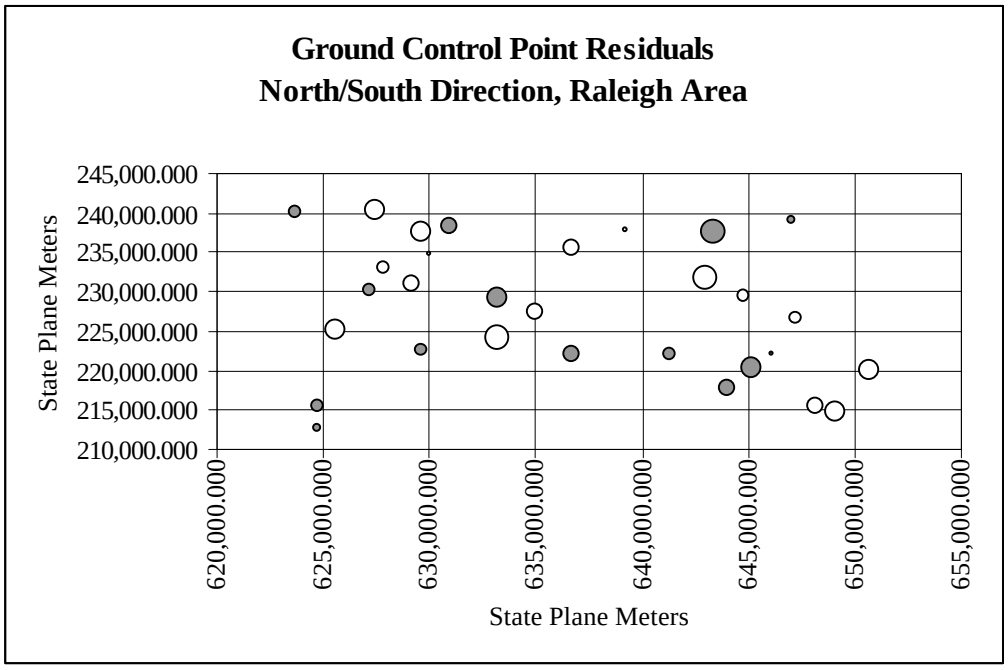

Figure 3.4: Distribution and magnitude of North/South residuals for the Raleigh area

Once we decided that the ground control points, transformation matrices, and the RMS errors were acceptable we shifted the coordinates for the 1988 images using the transformation coefficients given in tables 3.1 and 3.2. Since our subset images are relatively small sections of the original Landsat TM scenes we thought that the simple "shifting" resulting from the nearest neighbor resampling method would be appropriate to match the 1988 images to the 1994 images (Jensen, 1996, p. 129). However, it should be noted that the data were acquired from Eosat as geometrically corrected, which implies that there has been some resampling and our image data are not the original radiance values.

After conducting the nearest neighbor resampling, the resulting transformed coastal and Raleigh 1988 images were viewed simultaneously with their corresponding 1994 images using the “Blend/Fade”, “Swipe”, and “Flicker” utilities in the Imagine™ viewer. These utilities provide the user different display methods to switch between two images displayed on one area of the computer screen. Visually, the geometric registration of both the Raleigh and coastal scenes was quite satisfactory. Even with careful examination throughout the images there did not appear to be any shift or obvious misregistration for either scene.

Geometric rectification of digital orthophotos to 1994 Thematic Mapper imagery

As mentioned at the beginning of this section, we followed the logic of Earth Satellite Corporation (FGDC, 1992) and the recommendations of the C-CAP protocol (Dobson *et al.*, 1995, p. 15) by checking the Digital Orthophoto Quarter Quadrangles (DOQs) against our “master” 1994 images. The differences in pixel size (1 meter for the DOQ and 28.5 for the Landsat TM data) make it impossible to match one pixel from a DOQ to a pixel from the TM data. As discussed in Chapter 2, the DOQs meet horizontal National Map Accuracy Standards (NMAS). These specify that “90% of the well-defined points tested must fall within 40 feet.” (USGS, no date). This implies that a given DOQ is accurate to about a half of a TM pixel (45.25’ = ½ * 93.5’; where 93.5’ is an approximation for the

number of feet in a 28.5 meter pixel). Once the DOQs were brought into Imagine™, they were viewed against the 1994 TM imagery, again using the "Blend/Fade", "Swipe", and "Flicker" utilities. Visual inspection showed the DOQ to be closely registered to the TM data and matched the published sub-pixel accuracy standard

Geometric rectification of ancillary data

The use of the Croatan Forest GIS layer, the Natural Heritage Areas, and the Cary zoning map is to assess the usefulness of the proposed change detection method. When using these ancillary data we will be looking at polygon areas to check for change. These GIS layers will not be used to derive any of the quantitative modeling data. Instead they will be used for display and interpretation of the modeling results. Simultaneously viewing the ancillary data with image data show that the geometric agreement is appropriate for the interpretive purposes these data. The examples that use the GIS layers are presented in Chapter 8.

Essential results of geometric correction

The results of the geometric correction were satisfying. Using the image-to-image registration, as recommended by the C-CAP Protocol (Dobson *et al.*, 1995, p. 15) and using a first order, affine, transformation, we obtained RMS error below the recommended half pixel (see tables 3.1 and 3.2). The ground control points represent uniform and complete coverage over the two study areas and the RMS errors for each point do not show any spatial trend (see figures 3.1 through 3.4). To maintain the original digital numbers and avoid blurring the data, a nearest neighbor resampling method was used. The resulting transformed 1988 images were each viewed simultaneously with their corresponding 1994 image. Visual inspection indicated proper geometric registration.

Radiometric Correction

Background

In this section we describe the method used to radiometrically normalize the digital numbers from the 1988 images to the digital numbers from the corresponding 1994 images. We then transform the digital numbers to reflectance values using the sensor bias and gain calibration constants from the header file of the 1994 images.

The importance of radiometric correction is well established and described in many remote sensing textbooks (Jensen, 1996; Lillesand and Keifer, 1994; Richards, 1993), reports (Khorram *et al*., in press), and articles relating to image-based change detection (see the review article by Coppin and Bauer, 1996). The basic idea behind a radiometric correction is for differences in image data to represent actual differences in ground cover and not differences in atmospheric conditions and/or differences in the sensor.

There are many methods that can be use to conduct radiometric normalization. Two general classes for these methods are 1) correction based on modeling the physical environment and 2) corrections using empirical adjustments based on scene comparisons. Empirical methods use only the image data and normalize one scene to another (Morisette *et al.*, 1996). Corrections based on physical modeling generally use a radiative transfer model. (For example see Turner and Spencer, 1972, which Forester *et al.*, 1984, apply to Landsat MSS data. For a recent description and review of radiometric correction models, see Chavez, 1996). Because atmospheric data needed for physical model-based corrections are often difficult or impossible to obtain (Eckhardt, 1990) and highly detailed corrections may not be necessary (Richard, 1993, section 2.2.2), empirical corrections may be the preferred or only method of normalization. Also, some of the assumptions upon which the modeling is based (e.g. a diffuse, or Lambertian, surface) either may not be valid or may be impossible to check. Based on visual inspection, Eckhardt *et al.* (1990) find the empirical method superior to the deterministic approach. Furthermore, the C-CAP protocol suggests using empirical normalization techniques (Dobson *et al.*, 1995, p.

15). In keeping consistent with this protocol we decided to use an empirical approach. Additional support for this decision is based on two primary factors:

1. the atmospheric data needed for a model-base correction were not available
2. an empirical, image-based, approach will make the proposed change detection method more easily implemented by the general user

The first point is often the case for studies dealing with historical data; this fact provided justification for the second point.

Although we agree with C-CAP in its recommendation to use an empirical method for normalization, we will not use the "image regression" method (Eckhardt, *et al*., 1990) suggested in the protocol (Dobson, 1995, p. 15). Instead we will use the method described by Hall *et al.* (1991), which they refer to as "radiometric rectification". This method compares extremes in the distributions of the tassel-cap transformation band 1, representing brightness, and band 2, representing greenness (Kauth and Thomas, 1976; Crist and Cicone, 1984). A subset of pixels with low brightness and low greenness are selected from each image. Another set of pixels is selected with low greenness and high brightness values. Hall *et al.* (1991) refers to each of these two sets of pixels as coming from the non-vegetated extremes and they are referred to as the "radiometric control sets". Because the two sets of pixels are selected relative to their own brightness/greenness distribution, the set of pixels from each image do not necessarily represent the same ground area. The average values from the original TM band for these two subsets of pixels are then used to transform the 1988 image to the 1994 image based on the equation:

$$DN_{i-New} = m_i DN_{i-Old} + b_i \quad ;$$
$$\textit{where} \quad m_i = (B_{Ri} - D_{Ri}) / (B_{Si} - D_{Si}) \qquad \textbf{(eq. 3.2)}$$
$$\textit{and} \quad b = (D_{Ri} B_{Si} - D_{Si} B_{Ri}) / (B_{Si} - D_{Si})$$

DN_i represents the digital numbers from the subject image and "New" is the DN value after the transformation and "Old" is the original DN value. D_{si}, D_{Ri}, B_{si}, and B_{Ri} are, respectively, the means of the dark (D) and bright (B) radiometric control sets in the ith

band of the un-transformed subject image (***S***) and the reference image (***R***) (Hall *et al.*, 1991).

There are several reasons for using "radiometric rectification" instead of image regression which compares the same pixels from both images from manually selected "targets" (Eckhardt *et al.*, 1990, p. 1517). Some reasons, as stated by Hall *et al.*, are:

> A "fixed pixel" approach would in fact introduce several problems. Image misregistration causes pixels to shift spatially between acquisition; pixels which fell on linear or small features could consist of entirely different landscape materials from one acquisition to the next. In addition, road and rock outcrops can be overgrown after several years, and fixed points within water bodies change reflectance with changes in factors such as turbidity, sun glint, and aquatic vegetation. Finally, using fixed elements inevitably requires manual selection of sufficient numbers of image-to-image pairs of suitable pixels, which can be prohibitively labor intensive, particularly when several images from a number of years are being considered. (Hall, *et al.*, 1991, p. 13, footnote #1)

Although the misregistration issue has been minimized through the geometric correction described in section 3.1, two images can never be exactly corrected and, so, effects of misregistration will always be an issue. While the issue of linear features can be addressed by the careful selection of target sites, both this and the final point stated by Hall *et al.* (1991) relate to our concern about making the preprocessing as standard as possible.

Further justification for using their method is that Hall *et al.* (1991) showed their method to be appropriate for normalizing one scene to another then applying the atmospheric correction or sensor calibration of the "master" image to both images. By using the method of Hall *et al.*, we radiometrically rectify the 1988 images to the 1994 images then transform both sets of data from digital numbers to reflectance values using the sensor calibration constants from the 1994 images' header files. The transformation from digital numbers to reflectance values is suggested as part of radiometric correction (Chavez, 1996; Richards, 1993; Jensen, 1996; Caselles and Garcia, 1989). Sensor calibration coefficients are used to convert the radiance observed by the sensor into the digital numbers that make up the image. By using the sensor calibration numbers it is possible to

convert the digital numbers back to radiance values (Eosat, 1994). Unlike digital numbers, the radiance values are sensor-independent and have a physical meaning of spectral radiance which can be compared for different sensor and different studies (Price, 1987). However, the sensor calibration can drift over time (Thome *et al.*, 1993). This is what presumably led Eosat to do scene-specific bias and gain calibration. These numbers are included as part of the TM header file information (see Appendix A) for the 1994 data but not for the 1988 data. By using Hall's method we can use the more specific 1994 calibration constants to convert *both* the 1994 and 1988 digital number to at-sensor reflectance values. If deemed necessary for future studies, Hall *et al.*'s method can be used to normalize the image data from this study to a future image for which the necessary atmospheric data can be collected and a model-based atmospheric correction can be applied. The method will also permit future work from this study to be used in conjunction with data from other sensors.

Other possible empirical methods for radiometric correction are histogram matching and statistical normalization (see Morisette *et al.*, 1996, for an overview of these two methods as well as an overview of image regression). Histogram matching does not provide a one-to-one transformation and will degrade the radiometric resolution of the data. The statistical normalization is based on the assumption that the true average values for each band will remain constant for each date. This may be a safe assumption for a large area with a relatively small percentage of change. However, for smaller scenes there may be trends which effect the average value of the entire scene; these trends will be confounded with the radiometric correction. For example, in the Raleigh scene, it is possible that between 1988 and 1994 there was an increase in area covered by constructed features. This would cause a general increase in the mean reflectance values. In this case, using the statistical normalization would force the average values of each band to be the same and thus confuse the radiometric correction with actual change. Hall *et al.*'s (1991) radiometric rectification method only assumes that each image will have non-vegetated pixels which will show up in the extremes of the distribution of the brightness and greenness values and that *these* reflectance values should be the same from one date to the

next (although it does not assume that they are from the same ground area for each time period). The main concern about using their method, as stated by Hall *et al.* (1991) is the assumption that the transformation is linear and homogeneous across the scene. These are important considerations although they are also assumptions made in the other empirical-based methods. However, a linear transform -- using an additive and multiplicative term -- has the theoretical justification that the solar irradiance, downwelled sky radiance, and atmospheric transmission result in a multiplicative term while the path radiance results in an additive terms (Schott *et al.*, 1988). This theoretical justification for a linear transformation can be described with the equation:

$$\textit{At sensor radiance} = m \times \textit{ground radiance} + b \qquad \textbf{(eq. 3.3)}$$

where ***m*** accounts for solar irradiance, downwelled sky radiance, and atmospheric transmission and ***b*** accounts for path radiance.

In addition, a uniform transformation over the image is not a bold assumption for a 1024 by 1024 image. Because the assumptions are either minor or justified by theory we decided Hall *et al.*'s (1991) method would be suitable. Due to its advantages over the regression approach, histogram matching, and statistical normalization we decided radiometric rectification would be the best empirical method to use.

Radiometric Correction results

In this section we describe the specific calculations and correction applied to our image data. The first step was to do a "tassel cap" transformation to each image. This was done within Imagine™ using the coefficients associated with Landsat TM 5 (see table 3.6). After this we use Imagine™ to view the distribution of the brightness and greenness values for each image by using the "Create Feature Space Image" under the "Classification" menu. From these viewers, using an inquire cursor, we selected the threshold values for each image (as described in Hall *et al.*, 1991, pp. 14-15). The feature space images with boxes over the dark target and bright target subset areas are shown in

figures 3.5 and 3.6. The threshold values from the brightness and greenness values were used to select a subset of pixels from the original TM data. The average values of each original TM band were calculated from these subsets and equation 3.2 was used to compute the transformation. The threshold values, the number of pixels in each subset, the average value of the original TM six-band data for each subset, and the results of applying equation two to these values are presented in table 3.7 and 3.8. The reader may notice the number of pixels in the dark areas for the 1988 coastal scene is nearly twice as much as the dark areas for the 1994 coastal scene. As a check, we increased the threshold values for the 1994 scene by one integer. This resulted in the 1994 scene subset containing 1449 pixels. The average valued of the original TM bands for this larger subset did not change for the first two significant digits. With this we concluded that the method was fairly robust to slight changes in the threshold values and decided to stay with the original values even if the 1998 subset contains nearly twice as many points. The multiplicative and additive terms were then applied to the 1988 image. This completed the image normalization.

Table 3.6: Coefficients for the tassel-cap transformation

Band 1	Band 2	Band3	Band 4	Band 5	Band 6	Additive
0.2909	0.2493	0.4806	0.5568	0.4438	0.1706	10.3695
-0.2728	-0.2174	-0.5508	0.7221	0.0733	-0.1648	-0.731
0.1446	0.1761	0.3322	0.3396	-0.621	-0.4186	-3.3828
0.8461	-0.0731	-0.464	-0.0032	-0.0492	0.0119	0.7879
0.0549	-0.0232	0.0339	-0.1937	0.4162	-0.7823	-2.475
0.1186	-0.8069	0.4094	0.0571	-0.0228	-0.022	-0.0336

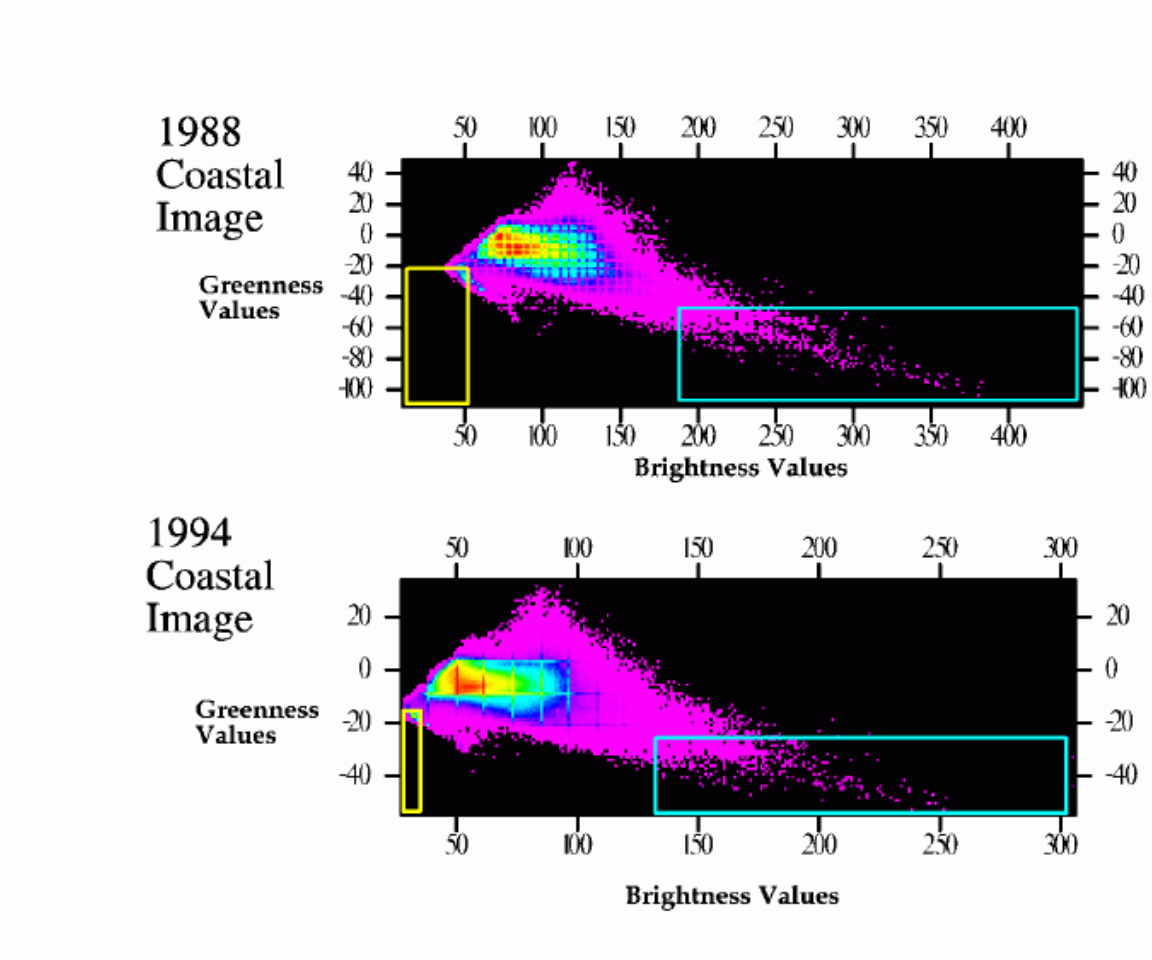

Plots show the two dimensional feature space:

X axis is the distribution of tassel-cap band one
Y axis is the distribution of tassel-cap band two
Colors represent frequency with magenta being the lowest and red being the highest

Yellow boxes are the dark non-vegetated subsets
Blue boxes are the bright non-vegetated subsets

Figure 3.5: Distribution of brightness and greenness values for the coastal area

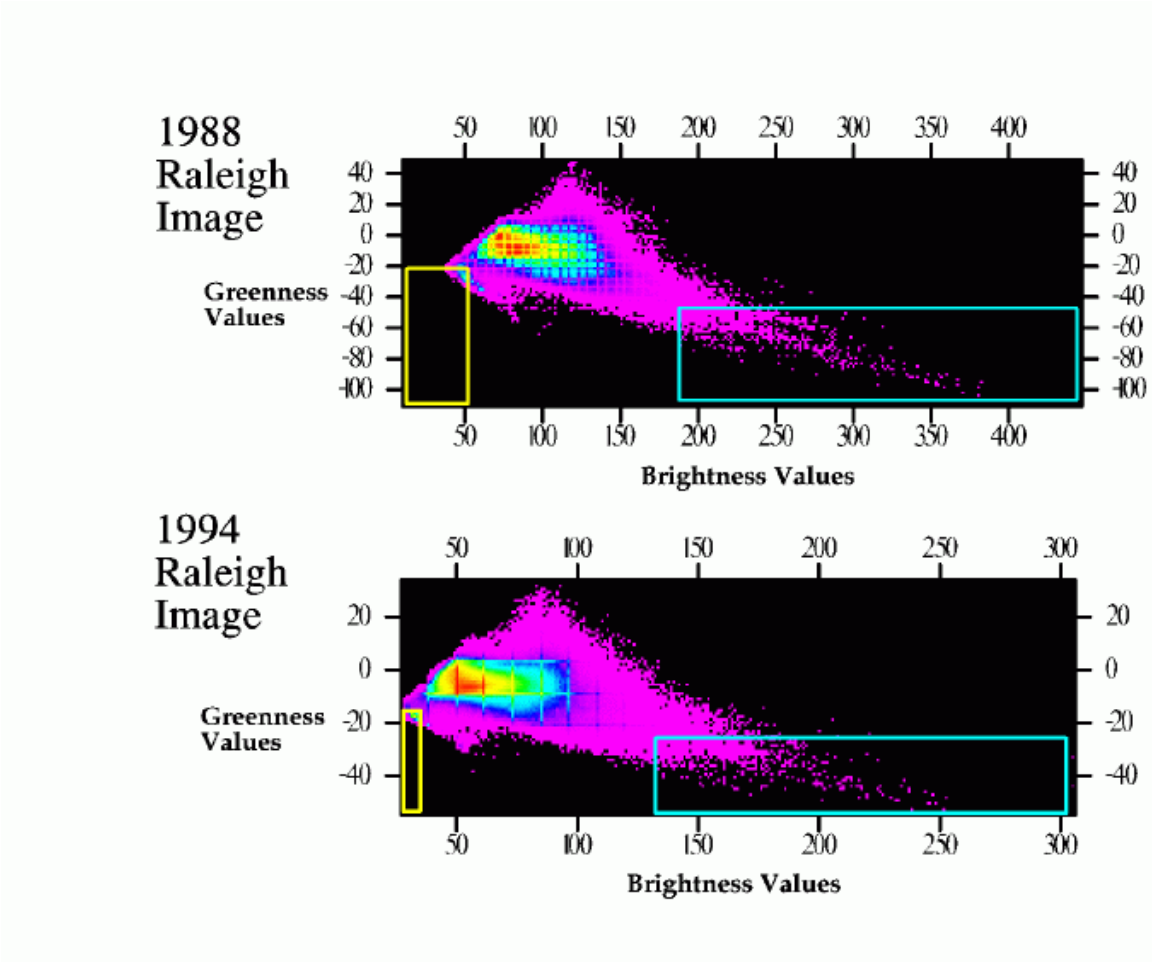

Plots show the two dimensional feature space:

X axis is the distribution of tassel-cap band one
Y axis is the distribution of tassel-cap band two
Colors represent frequency with magenta being the lowest and red being the highest

Yellow boxes are the dark non-vegetated subsets
Blue boxes are the bright non-vegetated subsets

Figure 3.6: Distribution of brightness and greenness values for the Raleigh area

Table 3.7: Threshold values and resulting transformation for the coastal scenes

Threshold Values:			**Average Values:**		
	Dark Objects	Bright Objects	Band #	Dark Objects	Bright Objects
1988 Image			1	52.174	130.411
Brightness	<43	>166	2	17.754	62.825
			3	15.449	84.471
Greenness	<-22	<-43	4	7.428	67.517
			5	2.261005	108.966
Number of pixels in subset:	7082	2570	6	1.730505	67.61
1994 Image			1	40.623	92.961
Brightness	<33	>110	2	13.52	45.648
			3	10.416	54.491
Greenness	<-17	<-28	4	3.802	46.713
			5	0.879467	74.313
Number of pixels in subset:	3240	3451	6	0.849318	41.985

Resulting Coefficients:

	Multiplicative Term (m_i)	Additive Term (b_i)
Band 1	0.668967	5.720297
Band 2	0.712831	0.864401
Band 3	0.638565	0.550817
Band 4	0.714124	-1.50251
Band 5	0.688192	-0.67654
Band 6	0.624408	-0.23122

Table 3.8: Threshold values and resulting transformation for the Raleigh scenes

Threshold Values:			**Average Values:**		
	Dark Objects	Bright Objects	Band #	Dark Objects	Bright Objects
1988 Image			1	54.327	140.237
Brightness	<50	>184	2	22.402	70.959
			3	20.463	98.554
Greenness	<-23	<-45	4	8.244	77.576
			5	3.682821	117.194
Number of pixels in subset:	2565	1685	6	2.20177	70.045
1994 Image			1	35.241	89.705
Brightness	<32	>131	2	12.874	46.297
			3	10.471	59.038
Greenness	<-15	<-25	4	3.882	55.391
			5	1.474155	86.012
Number of pixels in subset:	2675	1613	6	0.76285	49.146

Resulting Coefficients:

	Multiplicative Term (m_i)	Additive Term (b_i)
Band 1	0.633966	0.799541
Band 2	0.688325	-2.54586
Band 3	0.621928	-2.25552
Band 4	0.742933	-2.24274
Band 5	0.744753	-1.26864
Band 6	0.713161	-0.80737

The next step was to transform the Digital Numbers to at-sensor spectral radiance values using the post-calibration dynamic range used in the image processing given in the 1994 header files (listed as the "Gains/Biases" in the header files, see Appendix A). These values were transformed to multiplicative and additive terms based on the formula given by Eosat (Yang, 1996). These equations were used to transform the digital numbers to at-sensor radiance values.

$$L_\lambda = Gain \times DN + Bias;$$

$$where Gain = \frac{\left(\frac{LMAX_\lambda}{254} - \frac{LMIN_\lambda}{255} \right)}{Bandwidth_\lambda} \qquad \textbf{(eq. 3.4)}$$

$$and\ Bias = LMIN_\lambda$$

Where

L is the at-sensor spectral radiance
Gain is the digital value radiance conversation factor
DN is the digital number
Bias is the zero radiance offset
LMAX is the upper limit of the post calibrations dynamic range
LMIN is the lower limit of the post calibration dynamic range
Bandwidth is the detector bandwidth, and
λ refers to the spectra range (or "band") (Yang, 1996).

LMAX and LMIN are contained in fields 21 through 33 of the Eosat "Fast Format" header file (reproduced in Appendix A). Applying these equations results in at-sensor spectral radiance values in units of $\frac{milliwatts}{cm^2 \bullet steradian \bullet micrometer}$.

This gives the image data values a physical interpretation of reflected energy – independent of the sensor. The bias and gain values, Bandwidth, and the additive and multiplicative terms resulting from using these equations are given in table 3.9 for the coastal scene and table 3.10 for the Raleigh scene. Multiplying each image by the "Gain" term and then adding the "Bias" term completed the radiometric preprocessing and resulted in normalized images of at-sensor reflectance values. The summary statistics of the radiance values for each band, for each image, are given in table 3.11 for the coastal scene and table 3.12 for the Raleigh scene. The histograms are shown in figures 3.7 through 3.10. From the histograms and summary statistics it is seen that the two dates now show more similarity than before applying the radiometric rectification. (See Appendix B for the summary statistics and distribution of the original image data.) Although there are still differences in the mean values, and the extremes, we believe that the differences are mainly due to actual differences in ground cover reflectance. We

believe the rectified 1988 radiance values can be directly compared to the 1994 image. One reason for converting to radiance value is so these images will be comparable to other remotely sensed data, which does not necessarily have to be Landsat TM data. In addition to having two images we can compare to each other, by having the data as radiance values our images can be compared to other images in the future. It is worth noting that there are negative radiance values for some scenes, for some bands. The best explanation for this would be either measurement or sensor calibration error. In all cases, except "band 2" for the Raleigh scene, the minimum is different from zero by only a fraction of the standard deviation. For these we can consider the difference to be from measurement error. For "band 2" from the Raleigh scene, the minimum value is less than zero by about one standard deviation for both the 1988 and 1994 scene. This may be due to errors in sensor calibration. (Recall that the calibration from the 1994 scene was used for both the 1988 and 1994 images, which does not solve the problem but at least makes it consistent between scenes.) We decided to leave the negative numbers, as they were to maintain their relation to other values. However, the interpretation will be that negative values represent zero radiance.

Table 3.9: Bias and gain corrections for the coastal images

Band #	Min	Max	Bandwidth		Gain	Bias
1	-0.00734	1.05552	0.066		0.0633996	-0.1112121
2	-0.01515	2.60535	0.082		0.1258134	-0.1847561
3	-0.01171	1.63527	0.067		0.096776	-0.1747761
4	-0.02341	2.944	0.128		0.0912684	-0.1828906
5	-0.00562	0.68571	0.217		0.0125423	-0.0258986
6	-0.00314	0.42584	0.252		0.0067018	-0.0124603

Min = Lower limit of the post calibration dynamic range
Max = Upper limit of the post calibration dynamic range

Table 3.10: Bias and gain corrections for the Raleigh images

Band #	Min	Max	Bandwidth		Gain	Bias
1	-0.00757	1.0556	0.066		0.0634181	-0.114697
2	-0.01612	2.60574	0.082		0.1258785	-0.1965854
3	-0.01227	1.63562	0.067		0.0968294	-0.1831343
4	-0.02341	2.94483	0.128		0.0912939	-0.1828906
5	-0.00547	0.68584	0.217		0.012542	-0.0252074
6	-0.00313	0.42584	0.252		0.0067016	-0.0124206

Min = Lower limit of the post calibration dynamic range
Max = Upper limit of the post calibration dynamic range

Table 3.11: Mean and standard deviation radiance values for the coastal scene

Band 1

Summary Statistics	1988 Subset	1994 Subset
Minimum	0.2058	2.1078
Maximum	10.54	10.9204
Mean	2.663	2.7138
Median	2.5471	2.5897
Mode	2.4664	2.4865
Standard Deviation	0.362	0.3751

Band 2

Summary Statistics	1988 Subset	1994 Subset
Minimum	-0.1848	1.0734
Maximum	11.1384	11.5158
Mean	1.8375	1.8729
Median	1.6729	1.6852
Mode	1.6729	1.6852
Standard Deviation	0.4372	0.4386

Band 3

Summary Statistics	1988 Subset	1994 Subset
Minimum	-0.1748	0.5027
Maximum	12.2125	10.9545
Mean	1.2043	1.2228
Median	0.9865	1.0742
Mode	0.9865	0.8701
Standard Deviation	0.5173	0.5012

Band 4

Summary Statistics	1988 Subset	1994 Subset
Minimum	-0.2742	-0.0004
Maximum	11.1343	9.0352
Mean	1.9642	2.3497
Median	2.266	2.7174
Mode	0.1715	0.1761
Standard Deviation	0.9853	1.1747

Band 5

Summary Statistics	1988 Subset	1994 Subset
Minimum	-0.0259	-0.0259
Maximum	2.0686	2.4449
Mean	0.2473	0.2962
Median	0.2114	0.2829
Mode	0.1868	-0.0066
Standard Deviation	0.1936	0.2024

Band 6

Summary Statistics	1988 Subset	1994 Subset
Minimum	-0.0125	-0.0125
Maximum	1.0129	1.0129
Mean	0.0391	0.0461
Median	0.0276	0.0316
Mode	0.0116	0.0316
Standard Deviation	0.0479	0.047

Table 3.12: Mean and standard deviation radiance values for the Raleigh scene

Band 1

Summary Statistics	1988 Subset	1994 Subset
Minimum	-0.1147	1.6605
Maximum	10.1561	10.3463
Mean	2.1731	2.288
Median	2.0919	2.1355
Mode	1.9716	2.1016
Standard Deviation	0.3618	0.3659

Band 2

Summary Statistics	1988 Subset	1994 Subset
Minimum	-0.4483	0.6846
Maximum	14.7829	11.0066
Mean	1.3928	1.5456
Median	1.1581	1.2894
Mode	1.1581	1.1684
Standard Deviation	0.4915	0.506

Band 3

Summary Statistics	1988 Subset	1994 Subset
Minimum	-0.3768	0.3978
Maximum	14.0507	13.0824
Mean	1.1286	1.2312
Median	0.9758	1.042
Mode	0.5813	0.8438
Standard Deviation	0.576	0.5953

Band 4

Summary Statistics	1988 Subset	1994 Subset
Minimum	-0.3655	-0.0916
Maximum	11.9592	13.6938
Mean	2.131	1.9577
Median	2.0898	1.9008
Mode	1.8973	1.6316
Standard Deviation	0.6407	0.6465

Band 5

Summary Statistics	1988 Subset	1994 Subset
Minimum	-0.0378	-0.0252
Maximum	2.3327	2.4205
Mean	0.3901	0.382
Median	0.3697	0.3474
Mode	0.3419	0.3092
Standard Deviation	0.1654	0.1807

Band 6

Summary Statistics	1988 Subset	1994 Subset
Minimum	-0.0124	-0.0124
Maximum	1.1604	0.8387
Mean	-0.0748	0.0813
Median	0.0655	0.0674
Mode	0.0655	0.0607
Standard Deviation	0.0457	0.0506

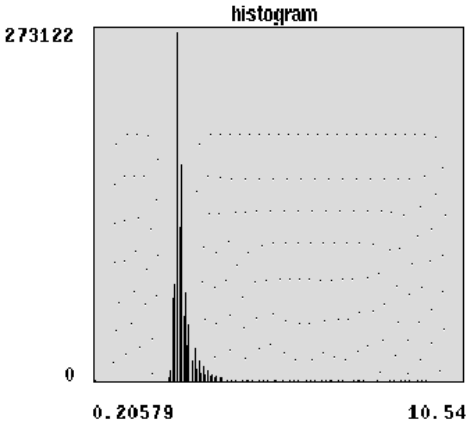

Band 1, 1988

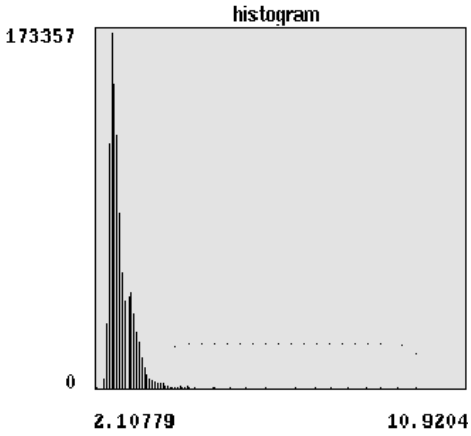

Band 1, 1994

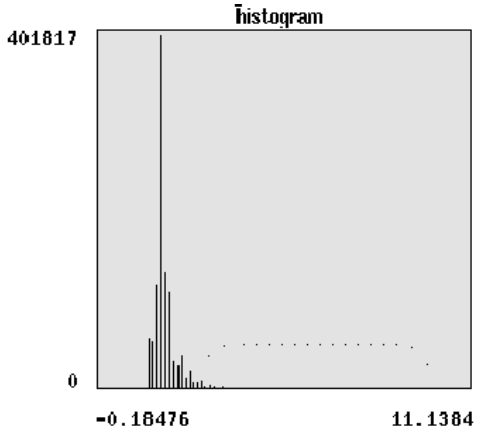

Band 2, 1988

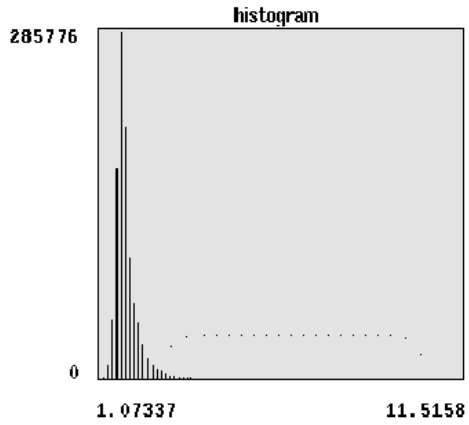

Band 2, 1994

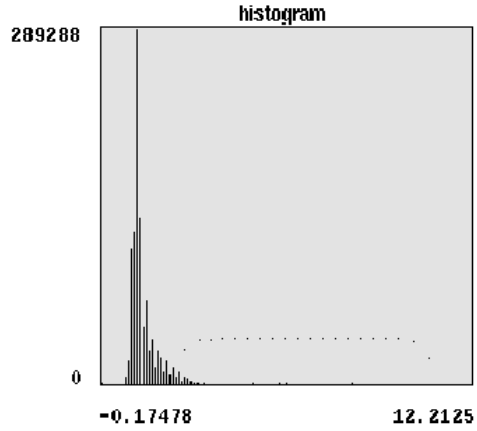

Band 3, 1988

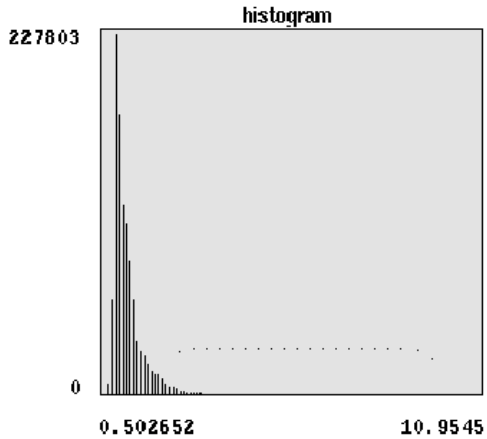

Band 4, 1994

Figure 3.7: Histograms of radiance values for the coastal area images

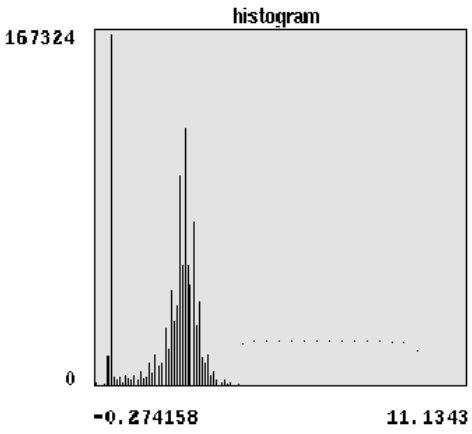

Band 4, 1988

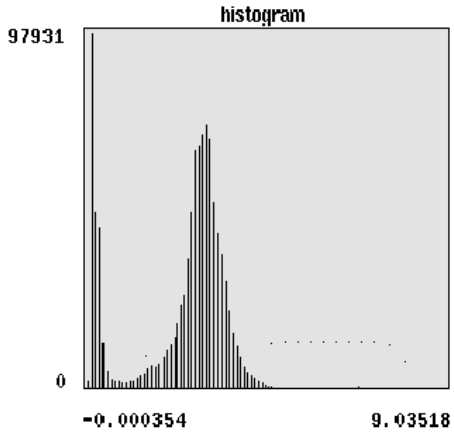

Band 4, 1994

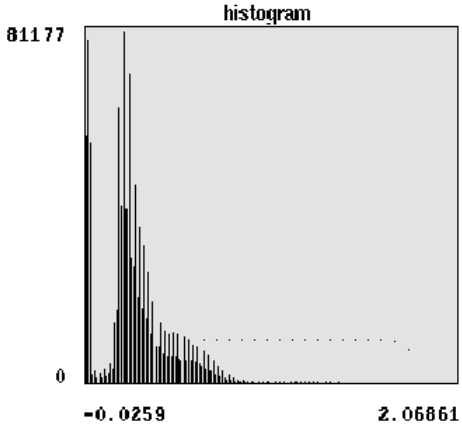

Band 5, 1988

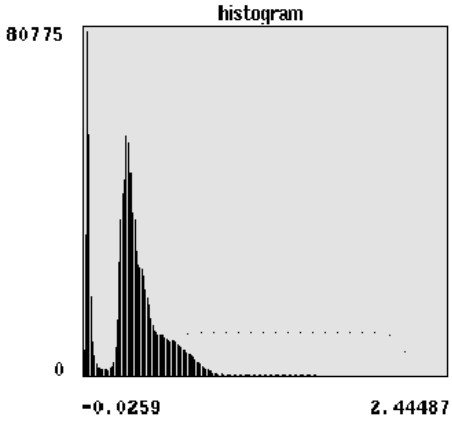

Band 5, 1994

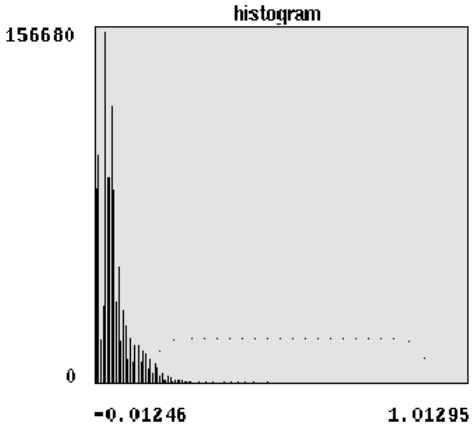

Band 6, 1988

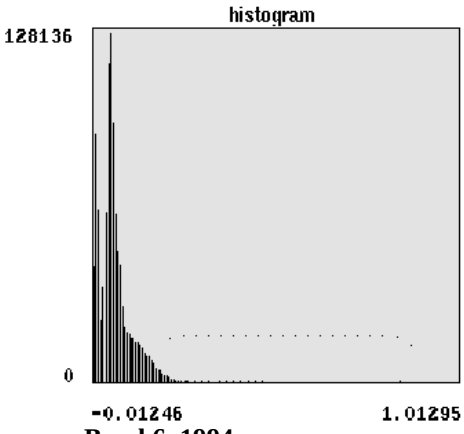

Band 6, 1994

Figure 3.7 (continued): Histograms of radiance values for the coastal area images

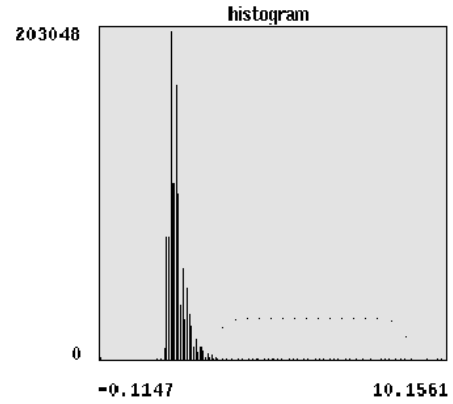

Band 1, 1988

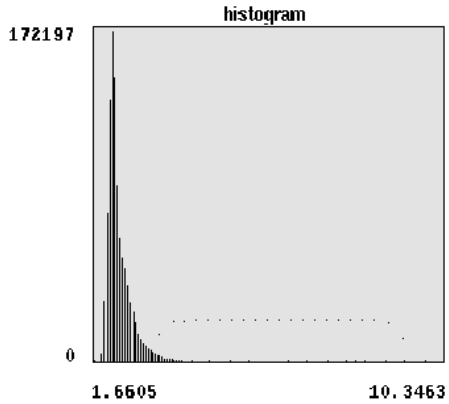

Band 1, 1994

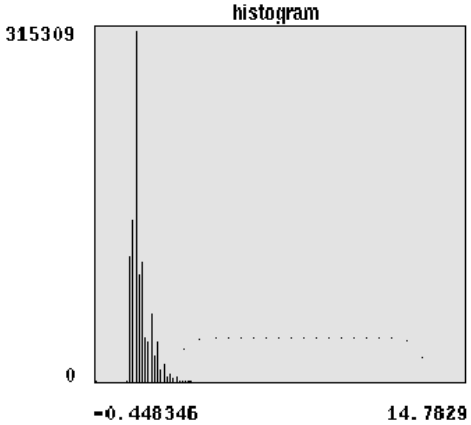

Band 2, 1988

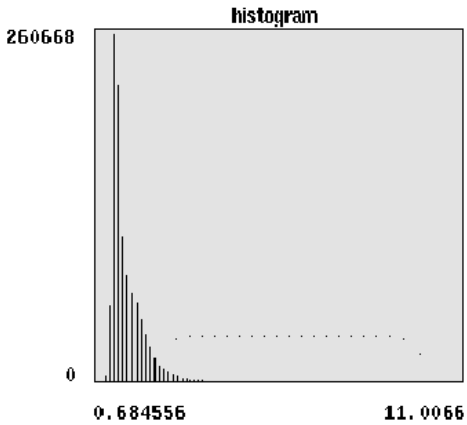

Band 2, 1994

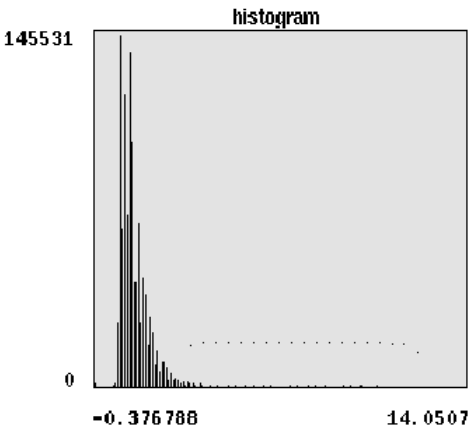

Band 3, 1988

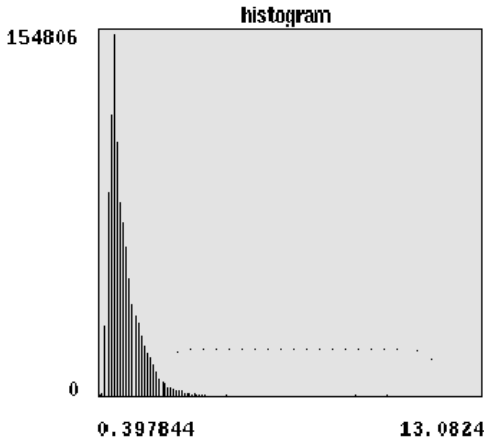

Band 3, 1994

Figure 3.8: Histogram of radiance values for the Raleigh area images

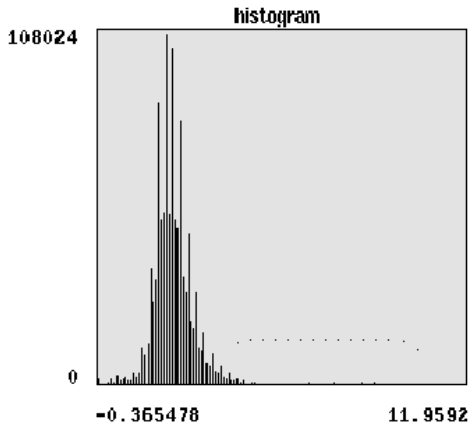

Band 4, 1988

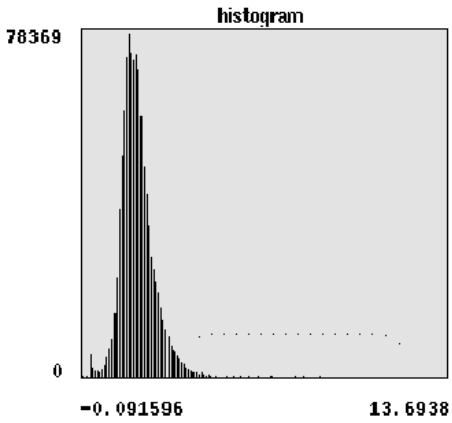

Band 4, 1994

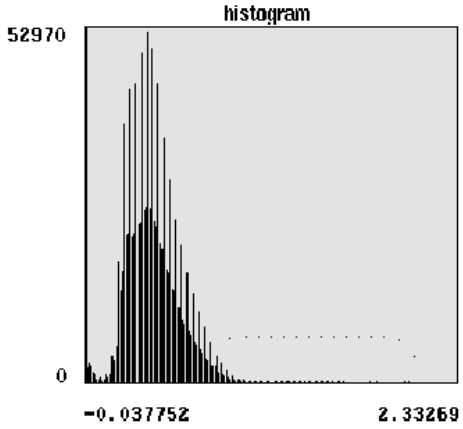

Band 5, 1988

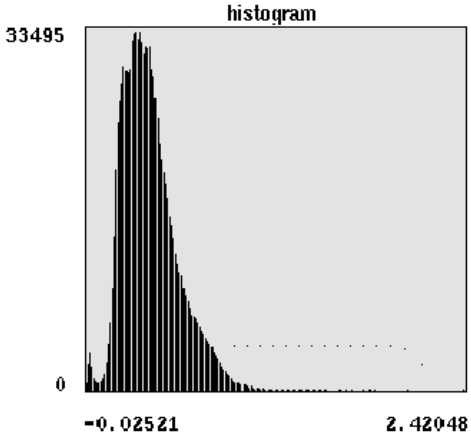

Band 5, 1994

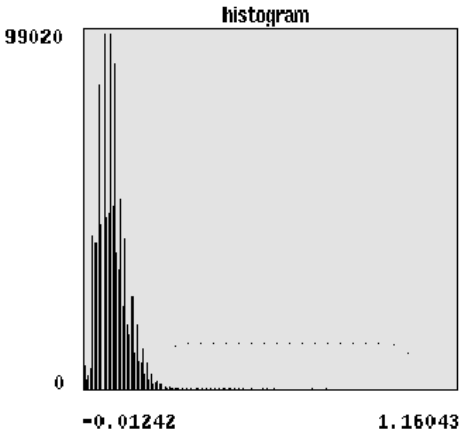

Band 6, 1988

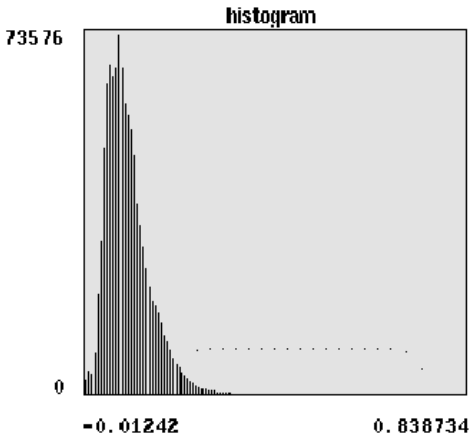

Band 6, 1994

Figure 3.8 (continued): Histograms of radiance values for the Raleigh area

Essential results of radiometric corrections

Using the method of Hall *et al.*(1991) and the header file information from the 1994 imagery we were able to first normalize the Digital Numbers of the 1988 data to the 1994 data and then transform both to spectral radiance values. This was based on our decision to do an empirical radiometric correction and the advantages of using Hall *et al.*'s method over other empirical methods. We do not have the historical atmospheric data to check our corrections. However, Hall *et al.* found their method to remove the effects of relative atmospheric differences to with 1% absolute reflectance (Hall *et al.*, 1991, p.26). We found the method robust to slight changes in the darkness and greenness threshold values. Additionally, the image statistics and histograms show the overall data sets have similar histograms and summary statistics. With this, we believe the radiometrically-corrected data will do well as input data into a change detection analysis. Through the process of radiometric correction we created two comparable images – comparable to each other and comparable to future images for possible future studies.